Biochemistry

Article

pubs.acs.org/biochemistry

Toward Allosterically Increased Catalytic Activity of Insulin-Degrading Enzyme against Amyloid Peptides

Igor V. Kurochkin,[†,∥] Enrico Guarnera,[†] Jin H. Wong,[†] Frank Eisenhaber,[†,‡,§] and Igor N. Berezovsky*[,†,‡]

[†]Bioinformatics Institute (BII), Agency for Science, Technology and Research (A*STAR), 30 Biopolis Street, #07-01, Matrix, Singapore 138671

[‡]Department of Biological Sciences (DBS), National University of Singapore (NUS), 8 Medical Drive, Singapore 117579

[§]School of Computer Engineering (SCE), Nanyang Technological University (NTU), 50 Nanyang Drive, Singapore 637553

Supporting Information

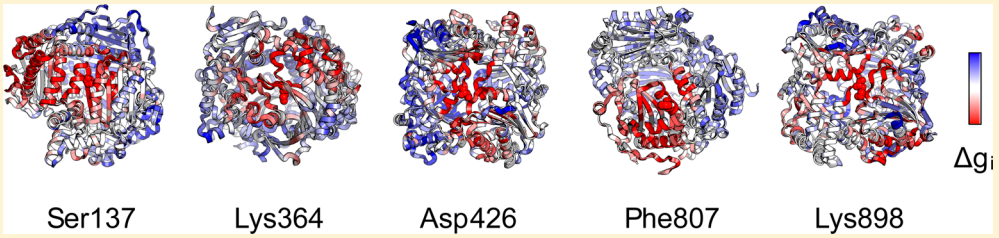

ABSTRACT: The physiological role of insulin-degrading enzyme (IDE) in the intracytosolic clearance of amyloid β (Aβ) and other amyloid-like peptides supports a hypothesis that human IDE hyperactivation could be therapeutically beneficial for the treatment of late-onset Alzheimer's disease (AD). The major challenge standing in the way of this goal is increasing the specific catalytic activity of IDE against the Aβ substrate. There were previous indications that the allosteric mode of IDE activity regulation could potentially provide a highly specific path toward degradation of amyloid-like peptides, while not dramatically affecting activity against other substrates. Recently developed theoretical concepts are used here to explore potential allosteric modulation of the IDE activity as a result of single-residue mutations. Five candidates are selected for experimental follow-up and allosteric free energy calculations: Ser137Ala, Lys396Ala, Asp426Ala, Phe807Ala, and Lys898Ala. Our experiments show that three mutations (Ser137Ala, Phe807Ala, and Lys898Ala) decrease the K_m of the Aβ substrate. Mutation Lys898Ala results in increased catalytic activity of IDE; on the other hand, Lys364Ala does not change the activity and Asp426Ala diminishes it. Quantifying effects of mutations in terms of allosteric free energy, we show that favorable mutations lead to stabilization of the catalytic sites and other function-relevant distal sites as well as increased dynamics of the IDE-N and IDE-C halves that allow efficient substrate entrance and cleavage. A possibility for intramolecular upregulation of IDE activity against amyloid peptides via allosteric mutations calls for further investigations in this direction. Ultimately, we are hopeful it will lead to the development of IDE-based drugs for the treatment of the late-onset form of AD characterized by an overall impairment of Aβ clearance.

Published in 1963, "Allosteric Proteins and Cellular Control System" marked a birth of a new area of research, which today is called allosteric regulation. On the basis of exclusively biochemical data on activity curves in the absence of any structural information at that time, Monod, Changeux, and Jacob[1] ingeniously foresaw in this work that "the absence of any inherent obligatory chemical analogy or reactivity between substrate and allosteric effector appears to be a fact of extreme biological importance". Since then, the fact that potential allosteric drugs are free from major drawbacks of traditional orthosteric compounds has been corroborated. For example, off-target inhibition and drug toxicity can be avoided in allosteric inhibition of protein kinases, as it does not affect nonspecifically conserved ATP-binding sites.[2] Allosteric modulators do not cause G protein-coupled receptor's desensitization typical of treatment with orthosteric activators, and at the same time, they provide functional selectivity of different subsets of downstream signaling pathways. It is noteworthy that just G protein-coupled receptors and protein kinases make up approximately half of the current drug targets.[2] The recently established omnipresence of the allosteric control[3] in all types of proteins[4,5] motivated numerous efforts to detect regulatory exosites and design effector molecules. By analogy with allosteric ligands, protein mutations that modulate protein activity by affecting its dynamics rather than directly changing catalytic and binding sites can be considered as allosteric.

In this work, we explore the insulin-degrading enzyme (IDE),[6] which is a Zn^{2+}-metalloprotease consisting of four structurally similar domains that have diverse sequences. An interface between the amino- and carboxyl-terminal halves

Received: August 1, 2016
Revised: November 22, 2016
Published: December 3, 2016

DOI: 10.1021/acs.biochem.6b00783
Biochemistry 2017, 56, 228−239

(IDE-N and IDE-C, including domains 1 and 2 and domains 3 and 4, respectively) forms a degradation chamber, and IDE undergoes a transition between open and closed conformations.[7] The catalytic activity of IDE was proposed to be allosterically regulated in a number of works.[7−16] It was found that, in addition to insulin,[6,17−21] IDE also degrades amylin, glucagon, hormones, and different growth factors and neurotransmitters.[14] Specifically, chemokines, calcitonin, atrial natriuretic factor, insulin-like growth factor II, transforming growth factor α, and β-endorphin are among the IDE substrates.[17] A large number of IDE substrates self-assemble as amyloid fibrils, and amyloid β (Aβ) peptide was one of the first natural substrates found to be degraded by IDE.[22] Comparison of the IDE structure in its free form with IDE bound to four different substrates revealed that both the N-terminal loop and the α-helical cleavage site in the substrates turn into β-strands.[7] To this end, an amyloidogenic determinant was proposed to serve as a substrate recognition motif of the protease,[23] implying that amyloidogenic peptides that possess various conformations in solution would assume a β-sheet conformation upon interaction with IDE.[24]

The finding that IDE degrades the Aβ peptide, which accumulates at abnormally high concentrations in the brain of Alzheimer's disease (AD) patients, stimulated interest in this protease and its therapeutic potential. The common late-onset form of AD is characterized by an overall impairment of Aβ clearance rather than Aβ overproduction.[25,26] Intraneuronal Aβ accumulation precedes extracellular Aβ deposition, and therefore, it is associated with cytotoxicity and neurodegeneration.[27] Though IDE was detected in different cellular compartments, such as peroxisomes, mitochondria, endosomes, and nucleus, as well as at the plasma membrane, in the extracellular vesicles and exosomes, it is primarily located in the cytosol.[14] In comparison to several proteases that are capable of degrading Aβ,[28] IDE was found to be the main peptidase that degrades cytoplasmic, monomeric Aβ.[29]

Additionally, a natural IDE gene variant characterized by an increased level of IDE expression was linked to the reduced plasma Aβ and reduced susceptibility to Alzheimer's disease, thus supporting a role for IDE in Aβ clearance in humans.[30] It was also observed that patients with type 2 diabetes have an increased risk of AD.[31,32] In a mouse model, it was demonstrated that even moderate transgenic overexpression of IDE in neurons effectively reduces the rate of accumulation of Aβ in the brain.[33] All this information suggests that pharmacological upregulation of IDE can have great potential in the treatment of AD, calling for further in-depth studies of IDE's function and its regulation.

Structural analysis of IDE revealed that the enzyme consists of two N-terminal (IDE-N) and C-terminal (IDE-C) halves linked by a short hinge loop that come together to form an enclosed catalytic chamber.[7] While the active form of IDE is a homodimer, the modulation of the protein's catalytic activity occurs intramolecularly.[9] The enzyme undergoes a conformational transition between open and closed states[34] during the binding of the substrate and release of the products.[7] It was shown, for example, that introduction of double-cysteine mutations into the contacts between IDE-N and IDE-C (D426C/K899C, N184C/Q828C, and S132C/E817C) leads to inactivation of IDE in the presence of the oxidizing agent, while under reduced conditions that destabilize the interface between IDE-N and IDE-C halves, all three double IDE mutants degraded fluorogenic substrate V, insulin, and Aβ_{1-42} more effectively.[7] Large substrates, such as Aβ_{40} and insulin, bind at both the active and so-called distal sites simultaneously, whereas short peptides bind only at the active or distal sites.[21] Allosteric regulation of the IDE activity can be driven by ATP/triphosphate/trinitrophenyl(TNP)-ATP,[9,11,13,14] anions, acrylation of cysteine residues,[10] and small molecules[35,36] such as somatostatin,[8] bradykynin,[18,37] and dynorphin[18,37] that bind to few distal sites.[15,16] It was hypothesized that allosteric activation by short peptides occurs because of a conformational change that destabilizes the N- and C-terminal domain interface.[15] In this case, it would allow a second molecule of the short substrate to bind to a distal site of the extended part of the substrate-binding site and increase the population of the enzyme in the open conformation.[34]

Here, we explore five mutations of IDE, which are anticipated to be allosteric on the basis of computational predictions and previous knowledge of the regulation of IDE activity against the Aβ substrate. In the experimental investigation of Aβ degradation, we detect a decrease in the K_m values for IDE^{S137A}, IDE^{F807A}, and IDE^{K898A} mutants along with an increase in IDE^{K898A} catalytic activity. We also analyze binding affinity and degradation of the short substrate, Abz-GGFLRKHGQ-EDDnp, demonstrating that IDE's activation is a result of intramolecular allosteric signaling. Using a recently developed structure-based statistical−mechanical model of allostery, we quantify effects of mutations in terms of allosteric free energy and link them to the changes in dynamics of IDE and its catalytic and regulatory sites.

MATERIALS AND METHODS

Computational Selection of Potential Mutation Targets. The selection of mutation targets was performed on the basis of (i) processing of the protein structure in the SPACER Web server[38] and detection of locations with increased binding leverage (eq 1), (ii) analysis of communication (ref 5 and eq 3) and interactions between the residues in detected locations and residues in known function-related binding sites, and (iii) analysis of literature aimed at identifying mutation targets of specific interest.

Binding leverage[39] allows one to quantify an effect of ligand binding on the overall protein dynamics, calculating the cost of binding site deformation when a ligand bound to a corresponding site resists the motion. First, Monte Carlo docking simulations that allow one to probe the protein surface are used for detecting the potential binding sites. Conformational changes are approximated by low-frequency C_α normal modes obtained using C_α elastic networks in the Molecular Modeling Toolkit (MMTK[40]) . The probe is modeled as a peptide with two to six C_α atoms. The binding leverage (L_A) for a set of normal modes A reads

$$L_A = \sum_{\mu \in A} \Delta U_\mu \tag{1}$$

where ΔU_μ is the total change in potential energy of a set of springs due to the motion of a normal mode μ. Springs of length d_{ij} are placed between all pairs of C_α atoms i and j, whose connecting line passes within 3.5 Å of any ligand atom (κ is an arbitrary spring constant), giving the following expression for ΔU:

$$\Delta U = \frac{k}{2} \sum_{ij} \Delta d_{ij}^2 \tag{2}$$

DOI: 10.1021/acs.biochem.6b00783
Biochemistry 2017, 56, 228−239

Leverage coupling provides a quantitative characteristic of allosteric communication[5] on the basis of the assumption that sites that have high binding leverage for the same motion are more likely to be allosterically coupled than sites that have high binding leverage for only motion along independent degrees of freedom {in the case of the IDE structure analyzed here [Protein Data Bank (PDB) accession code 2g54], we consider binding leverage values of >30}. The strength of communication between two sites, P and Q, is defined as a dot product of binding leverages of these sites (λ_P and λ_Q, respectively):

$$D_{PQ} = \lambda_P \cdot \lambda_Q \tag{3}$$

The vector of the binding leverage of site P is defined as $\boldsymbol{\lambda}_P = (\lambda^*_{P1}, \ldots, \lambda^*_{Pn})$, where $\lambda^*_{P\mu}$ is a binding leverage of site P caused by normal mode μ:

$$\lambda^*_{P\mu} = \frac{\sum_{i\in P} \lambda_{i\mu}}{\| P \|} \tag{4}$$

where the norm of P is the number of elements in the set.

The calculations were performed on five crystal structures (results are not shown, but they are available as downloadable data on the SPACER Web server upon starting the session with the corresponding PDB entry) under accession codes 2g54 (Zn21-IDE-insulin B chain), 2g56 (Zn21-free IDE-insulin B chain), 2g47 (IDE-Aβ_{40}), 2g48 (IDE-amylin), and 2g49 (IDE-glucagon). The probes with sizes of two, four, and six residues were used. The optimal probe size was found to be four residues (default value in the SPACER's "Binding Leverage" routine[38]). All results obtained on different structures and for different probe sizes are qualitatively consistent. Here, we use results obtained for the Zn21-IDE-insulin B chain structure (PDB accession code 2g54) structure to obtain a list of potential mutation targets (Table S1).

Five residues, Ser137 (binding leverage L_A = 38.0), Lys364 (L_A = 69.7), Asp426 (L_A = 38.5), Phe807 (L_A = 2.34), and Lys898 (L_A = 35.8), were mutated into Ala for experimental investigation of the potential allosteric effects.

Modeling the Allosteric Free Energy Caused by Mutations. To quantify the effects of allosteric signaling caused by mutations, we use here a specific implementation of a general structure-based statistical−mechanical model of allostery.[41] It is comprised of three major components: (i) the modeling of the dynamics in unperturbed (i.e., unligated/wild-type) and perturbed (i.e., ligated, mutated, modified, etc.) protein forms using normal modes, (ii) a per-residue allosteric potential used for the energy evaluation of the effects of structural changes caused by protein dynamics, and (iii) evaluation of a per-residue allosteric free energy, that is, the work exerted on the residue of interest as a result of allosteric signaling caused by a perturbation of the residue's structural environment. In this work, we are interested in characterizing the energetics of "allosteric mutations", namely sequence mutations that have an effect on the intrinsic functional dynamics of the protein. In the aforementioned structure-based statistical−mechanical model of allostery, proteins are described via the harmonic model.

The effect of a mutation is modeled by the extreme perturbation of the interactions of the mutated residue in the protein harmonic model that is used to calculate normal modes of the system. We define an effective harmonic potential for the elastic network representation of the wild-type and mutated proteins. The energy function of the wild-type protein is

$$E^{\mathrm{WT}}(\vec{r} - \vec{r}^{\,0}) = \sum_{\text{pairs } i,j} k_{ij}(d_{ij} - d_{ij}^{\,0})^2 \tag{5}$$

where $\vec{r}$ and $\vec{r}^{\,0}$ are the coordinates of the protein structure in generic and reference configurations, respectively, k_{ij} are spring constants of the protein harmonic model, and d_{ij} and $d_{ij}^{\,0}$ are interresidue distances in generic and reference protein configurations, respectively.

The energy function of the mutated protein is defined as

$$E^{\mathrm{MUT}}(\vec{r} - \vec{r}^{\,0}) = \sum_{i\neq \mathrm{MUT},j} k_{ij}(d_{ij} - d_{ij}^{\,0})^2 + \alpha \sum_{j} k_{\mathrm{MUT},j}(d_{ij} - d_{ij}^{\,0})^2 \tag{6}$$

The second term of eq 6 accounts for the effect of a point mutation, as a perturbation of the wild-type's energy function (eq 5). In particular, α is a perturbation parameter, which acts as a scaling factor of the force constant and reflects the type of mutation considered in the calculation (see below). If α = 1 in the equation for the mutated protein, the energy function of the mutated protein is identical to that of the wild type. When α is very small (10^{-5} in the work), the perturbation (mutation) results in a residue that interacts weakly with the rest of the protein, whereas the opposite (strong interactions between mutated residues and the rest of the protein) is obtained for large values of α (100 in this work).

The dynamics of the wild-type and mutated proteins are characterized by calculating the set of normal modes using Molecular Modeling Toolkit (MMTK[40]). These sets of normal modes are used as the input for the allosteric potential, the second component of the statistical−mechanical model mentioned above, which is defined as

$$U_i(\sigma) = \frac{1}{2} \sum_{\mu} \varepsilon_{\mu,i} \sigma_\mu^{\,2} \tag{7}$$

The allosteric potential evaluates the elastic work (in harmonic approximation) that is exerted on a particular residue as a direct result of the protein's dynamics, which is different in the wild-type and mutated structures and is reflected in corresponding normal modes e_μ^{WT} and e_μ^{MUT}, respectively. In general, this work is different in the wild type and in the mutated proteins for values of α substantially deviating from 1. The parameters ε in eq 7 depend on the normal modes of the wild-type and mutated proteins ($\varepsilon_{\mu,i}^{\mathrm{WT}}$ and $\varepsilon_{\mu,i}^{\mathrm{MUT}}$, respectively), and the coefficients σ_μ are Gaussian variables with the variance $1/\varepsilon_{\mu,i}$. The summation in eq 7 runs over the 10 lowest-frequency normal modes, which reflect the large-scale structural changes associated with regulation of the protein's activity.[39]

Finally, the per-residue allosteric free energies are obtained by comparing the configurational ensembles for the wild-type and mutated residues. The ensemble of configurations of a single residue is characterized by all possible displacements assumed by the neighboring residues, which are obtained from the linear combinations of the low-frequency normal modes for the wild-type and mutated proteins, respectively. The resulting allosteric free energy is

$$\Delta g_i^{\mathrm{MUT}} = \Delta g_i(\mathrm{WT} \rightarrow \mathrm{MUT}) = \frac{1}{2} k_{\mathrm{B}} T \sum_{\mu} \ln \frac{\varepsilon_{\mu,i}^{\mathrm{MUT}}}{\varepsilon_{\mu,i}^{\mathrm{WT}}} \tag{8}$$

with the summation running over the low-frequency modes, where k_{B} is the Boltzmann constant and T is the absolute

DOI: 10.1021/acs.biochem.6b00783
Biochemistry 2017, 56, 228−239

temperature. The values of $\Delta g_i(\mathrm{WT} \rightarrow \mathrm{MUT})$ calculated with eq 8 evaluate the difference in the amount of configurational work that was exerted on residue i as a result of the change in the protein dynamics caused by the mutation. It is important to note that while the allosteric potential evaluates the energetics of the single protein configuration, the free energy in eq 8 is the result of an exact statistical−mechanical calculation, in which the ensembles of configurations for wild-type and mutated structures are considered.[41] To complement the description of the effect of mutation at the single-residue level, we also characterize the effect of mutation on the overall stability of the protein.[42] We calculate the free energy changes of the entire protein upon mutation

$$\Delta g_i(\mathrm{WT} \rightarrow \mathrm{MUT}) = \frac{1}{2} k_B T \sum_{\mu} \ln \frac{\lambda_\mu^{\mathrm{MUT}}}{\lambda_\mu^{\mathrm{WT}}} \tag{9}$$

where e_μ^{WT} and e_μ^{MUT} are the eigenvalues of the Hessian matrix of the harmonic models representing the wild-type and mutated proteins,[42] respectively. This global free energy change is a crude estimate of the change in the structural stability of the whole protein as a result of mutation.

The allosteric free energies for the residues analyzed in this work were calculated in two extreme scenarios: the over-stabilizing mutations (UP mutation, force constant scaling factor $\alpha = 100$, $\Delta g_{\mathrm{residue}}^{\uparrow \mathrm{MUT}}$) and the contact-eliminating mutations (DOWN mutation, force constant scaling factor $\alpha = 10^{-5}$, $\Delta g_{\mathrm{residue}}^{\downarrow \mathrm{MUT}}$). Finally, the allosteric effect of a mutation is given as the difference between the effects of the UP and DOWN mutations, namely

$$\Delta\Delta g_{\mathrm{residue}}^{\mathrm{MUT}} = \Delta g_{\mathrm{residue}}^{\uparrow \mathrm{MUT}} - \Delta g_{\mathrm{residue}}^{\downarrow \mathrm{MUT}} \tag{10}$$

The meaning of the estimated allosteric free energy difference per residue is the quantification of the amount of coherent work a specific amino acid performs (i.e., the amount of work exerted in a particular position of the protein chain) as a result of the mutation of another residue in the protein structure. The allosteric free energy difference between UP mutations and DOWN mutations evaluates how the per-residue performed work changes upon comparing mutations leading to contact reinforcement (mutations that introduce the most bulky possible residue) and contact disruption (GLY-like mutation).

The calculated per-residue double allosteric free energy differences due to a mutation are used as an input to determine averaged per-site and per-domain allosteric free energies, that is

$$\Delta\Delta g_{\mathrm{site}}^{\mathrm{MUT}} = \langle \Delta\Delta g_{\mathrm{site}}^{\mathrm{MUT}} \rangle_{\mathrm{site}} \text{ and}$$
$$\Delta\Delta g_{\mathrm{domain}}^{\mathrm{MUT}} = \langle \Delta\Delta g_{\mathrm{domain}}^{\mathrm{MUT}} \rangle_{\mathrm{domain}} \tag{11}$$

where the averages are taken over the residues belonging to a site and to a domain. To estimate the global changes in protein stability caused by a mutation, we also calculate the allosteric free energy difference caused by UP and DOWN mutations:

$$\Delta\Delta g_{\mathrm{protein}}^{\mathrm{MUT}} = \Delta g_{\mathrm{protein}}^{\uparrow \mathrm{MUT}} - \Delta g_{\mathrm{protein}}^{\downarrow \mathrm{MUT}} \tag{12}$$

which is computed from the Hessian matrices of the protein harmonic model employed.[41]

Experimental Investigation of the Effect of Allosteric Mutations. *Fluorogenic Peptides.* Fluorogenic peptide FAM-Aβ_{1-40}-Lys-biotin (F-Aβ-B) was synthesized by New England Peptide, Inc. (Gardner, MA). Fluorescein-based fluorescent dye FAM was attached to the amino terminus via a peptide bond. Biotin was attached to the carboxyl-terminal lysine. The protocol of Ryan et al.[43] was used to dissolve of F-Aβ-B. Specifically, 5 mg of F-Aβ-B peptide was dissolved in 10 mL of 10% (w/v) NH_4OH (final concentration of 0.5 mg/mL) and then dispended into 20 × 0.5 mL low-protein binding tubes (Eppendorf LoBind Protein Tubes). They were incubated for 10 min at room temperature followed by sonication for 5 min in a water bath (ultrasonic cleaner, Branson Co.). NH_4OH was removed by lyophilization to yield a salt-free peptide. Aliquots were stored at −80 °C. Immediately prior to use, NH_4OH-treated F-Aβ-B peptide (0.25 mg in a tube) was dissolved in 60 mM NaOH to a stock concentration of 50 μM and sonicated for 5 min. The concentration of F-Aβ-B was verified by measuring the absorbance at 494 nm assuming a molar absorption coefficient for FAM of 70000 M^{-1} cm^{-1}.

Abz-GGFLRKHGQ-EDDnp was synthesized and purified by Sigma. It was dissolved in *N*,*N*-dimethylformamide (DMF), then diluted with water to a concentration of 5 mM in 20% DMF, and stored in aliquots at −80 °C. The concentration of Abz-GGFLRKHGQ-EDDnp prior to use was estimated from the measurement of the absorbance at 365 nm assuming a molar absorption coefficient for EDDnp of 17300 M^{-1} cm^{-1}.

Preparation of IDE Expression Constructs. The human IDE sequence starting from second initiation codon Met_{42} (NCBI Reference Sequence NP_004960.2), representing the major translational start site,[44] was amplified by polymerase chain reaction and cloned into the AscI−NotI cloning site in the pETDuet-1 plasmid vector that provides an N-terminal hexahistidine (His_6) tag. The human IDE containing S137A, K364A, D426A, F807A, and K898A mutations was obtained using the QuikChange II XL Site-Directed Mutagenesis Kit (Stratagene). Primers used for mutagenesis are listed in Table S2. All generated constructs were verified by sequencing of the full length IDE inserts.

Expression and Purification of Recombinant IDE. Expression and purification of recombinant IDE were performed by modification of the method described by Chesneau and Rosner.[45] BL21-CodonPlus (DE3)-RIPL competent cells (Strategene) were transformed with pETDuet-1 containing the wild-type IDE or pETDuet-1 IDE^{S137A}, IDE^{K364A}, IDE^{D426A}, IDE^{F807A}, and IDE^{K898A} encoding inserts. Cells were grown in Luria broth containing 50 μg/mL ampicillin and 50 μg/mL chloramphenicol at 37 °C until the OD_{600} of the culture reached 0.3−0.4. The expression of the recombinant IDEs was induced by adding IPTG to a final concentration of 50 μM. Cells were grown for 43 h at 15 °C and then harvested by centrifugation at 4500*g* and 4 °C. The pellets were stored at −80 °C until recombinant proteins were extracted and purified. All protein extraction and purification steps of the soluble recombinant IDEs were performed either on ice or at <4 °C.

The pellets were resuspended in extraction buffer [50 mM sodium phosphate (pH 8.0), 300 mM sodium chloride, and 1 mM β-mercaptoethanol] containing 0.1 mg/mL lysozyme and 1 tablet of cOmplete EDTA-free Protease Inhibitor Cocktail (Roche Diagnostics) for 50 mL of buffer. The cell suspension was incubated on ice for 30 min. Lysates were sonicated and centrifuged for 20 min at 15000*g*; 1 M of imidazole (pH 8.0) was added to the supernatants to a final concentration of 5 mM. The resulting soluble protein extract was applied to a 1 mL TALON metal affinity column (Clontech), pre-equilibrated with extraction buffer containing 10 mM imidazole (pH 8.0). Then, the column was washed with 20 volumes of equilibration

DOI: 10.1021/acs.biochem.6b00783
Biochemistry 2017, 56, 228−239

buffer and eluted with 7 volumes of elution buffer [50 mM sodium phosphate (pH 7.5), 300 mM sodium chloride, 1 mM β-mercaptoethanol, and 200 mM imidazole]. Fractions of 0.5 mL were collected and concentrated using a 10 kDa molecular weight cutoff concentrator (Amicon) and passed through a Superdex S200 10/300 gel filtration column (GE Healthcare) (Figure S1). Fractions of recombinant IDE corresponding to the dimeric form (shown as solid bars in Figure S1) were pooled and stored at −80 °C until further use for proteolytic assays. The purity of the IDE preparations was estimated by Coomassie staining of sodium dodecyl sulfate−polyacrylamide gel electrophoresis gels (Figure S2). The IDE concentration was determined using a NanoDrop 2000 UV−vis spectrophotometer.

F-Aβ-B Degradation Assay. The F-Aβ-B degradation assay was performed using the method of Leissring et al.[46] with minor modifications. The assay mixture (total volume of 50 μL) consisted of 5 μL of a 10× stock of F-Aβ-B in buffer A [50 mM HEPES, 100 mM NaCl, and 0.05% (w/v) bovine serum albumin (pH 7.7)]. The reaction was initiated by adding 1.5 ng of recombinant IDE in 25 μL of buffer A. Buffer A was added instead of IDE for a negative control. Incubation proceeded for 10 min at 37 °C. The reaction was stopped by adding 550 μL of 2 mM 1,10-phenanthroline in buffer A. Uncleaved F-Aβ-B was precipitated with 20 μL (packed volume) of Pierce High Capacity Streptavidin Agarose beads (ThermoFisher Scientific). After the tubes had been rocked for 1 h at 4 °C, the beads were centrifuged at 15000*g* for 15 min. The pellet represented uncleaved F-Aβ-B. The supernatant containing cleaved F-Aβ-B fragments was transferred to black, clear bottom polysterene 96-well plates (Corning, Inc.) and analyzed for fluorescence intensity (λ_{ex} = 485 nm, and λ_{em} = 528 nm) using a Synergy MX Multi-Mode Microplate Reader from BioTek.

Abz-GGFLRKHGQ-EDDnp Degradation Assay. The hydrolysis of the fluorogenic peptide Abz-GGFLRKHGQ-EDDnp was analyzed as described by Song et al.[37] Cleavage at any peptide bond leads to the separation of the quenching EDDnp (C-terminal fluorescence-quenching ethylenediamine-2,4-dinitrophenyl) group from the fluorescent Abz group and an increase in fluorescence. The Abz/EDDnp pair produces one of the best quencher effects, providing a large increase in fluorescence after substrate hydrolysis.[47,48] The assay mixture (total volume of 100 μL) consisted of 10 μL of a 10× stock of Abz-GGFLRKHGQ-EDDnp in 50 mM HEPES (pH 7.7) containing 100 mM NaCl and 20 ng of IDE (except 120 ng for IDE^{D426A}). The reaction proceeded for 40 min at 37 °C and was stopped by adding 50 μL of 6 mM 1,10-phenanthroline in 50 mM HEPES (pH 7.7) containing 100 mM NaCl. Then, the fluorescence was measured in black bottom polysterene 96-well plates (Corning, Inc.) (λ_{ex} = 318 nm, and λ_{em} = 419 nm). For measurements of Abz-GGFLRKHGQ-EDDnp concentrations, the total fluorescence change upon cleavage of known amounts of the fluorogenic peptide with excess trypsin was recorded.

Analysis of Kinetic Parameters. To estimate kinetic parameters K_m (Michaelis−Menten constant, the substrate concentration needed to achieve a half-maximal enzyme velocity) and V_{max} (maximal enzyme velocity), the initial velocity was plotted versus substrate concentration. Data were analyzed by nonlinear regression to the Michaelis−Menten equation, using GraphPad Prism 6 (GraphPad Software Inc., La Jolla, CA).

RESULTS

Pipeline of the Computational and Experimental Analysis. The procedure implemented in this work includes the following consecutive steps. First, we utilized the SPACER Web server (PDB accession code 2g54[7]) to obtain the list of amino acid residues that can allosterically modulate IDE's activity (Table S1) by affecting the overall protein's dynamics. From this set, we selected five sites for experimental verification of allosteric mutations on the basis of their involvement in the key stabilizing interactions and dynamics of the IDE structure. Specifically, Ser137 and Lys364 are involved in the interface between domains 1 and 2 (D1−D2), and their mutual dynamics is indicated in the high binding leverage of these residues. Lys364 is an immediate residue to the exosite involved in substrate binding. Asp426 and Lys898 are in the D2−D4 interface, also revealing high binding leverage. Phe807 is characterized by the extremely low binding leverage,[38] presumably being a local hydrophobic stabilizer of domain 4.

We started by testing the anticipated allosteric effects of mutations in six recombinant IDE proteins, including wild-type IDE (IDE^{WT}) and five mutants (IDE^{S137A}, IDE^{K364A}, IDE^{D426A}, IDE^{F807A}, and IDE^{K898A}). We examined the kinetic properties of the recombinant IDE forms during degradation of two previously well-studied substrates. These are the long FAM-Aβ_{1-40}-Lys-biotin (Aβ) peptide and the short synthetic peptide Abz-GGFLRKHGQ-EDDnp. Because short substrate peptides can presumably enter the catalytic site more easily than the long ones can, the comparison of their degradation kinetics allows us to confirm the allosteric mode of IDE's activity modulation. In addition, we calculated allosteric free energies as a result of mutations in four domains of IDE, as well as in the exosite, catalytic, substrate recognition, Zn^{2+}-binding sites. On the basis of experimental data and the quantitative estimates of the allosteric free energies associated with the corresponding mutations, we consider the intramolecular scenario of the IDE's allosteric regulation.

Effect of Mutations on the Catalytic Activity of IDE. *Experimental Analysis.* A characteristic feature of IDE is that it has two substrate-binding sites in the catalytic chamber: a catalytic cleft that coordinates a zinc ion and a distal site called an "exosite" that anchors the N-terminus of its peptide substrates.[7,14] In addition to Aβ, insulin, glucagon, amylin, and other peptides with molecular weights of 3−10 kDa, IDE also degrades peptide substrates that are too short to occupy both the catalytic site and the exosite simultaneously.[21] IDE typically has lower binding affinities for such substrates. During the proteolytic cycle, IDE undergoes a series of conformational changes from an open to fully closed conformational state. In the open state, IDE can bind both small and large substrates, such as Aβ, while the swinging door motion resulting in closed conformational state permits the entrance of only smaller peptides.[7,14]

The degradation of Aβ was assessed using a fluorescence-based assay described by Leissring et al.[46] To determine the saturation concentration of Aβ, kinetic parameters of degradation were assayed for the wild-type enzyme and three IDE variants, S137A, F807A, and K898A, in a range of the peptide concentrations between 0.25 and 8 μM. We found that the cleavage of Aβ by wild-type IDE and all IDE variants follows normal Michaelis−Menten kinetics and reaches the plateau at substrate concentrations of <2 μM (Figure S3). The mutated proteases showed decreased K_m and increased k_{cat}/K_m

DOI: 10.1021/acs.biochem.6b00783
Biochemistry 2017, 56, 228−239

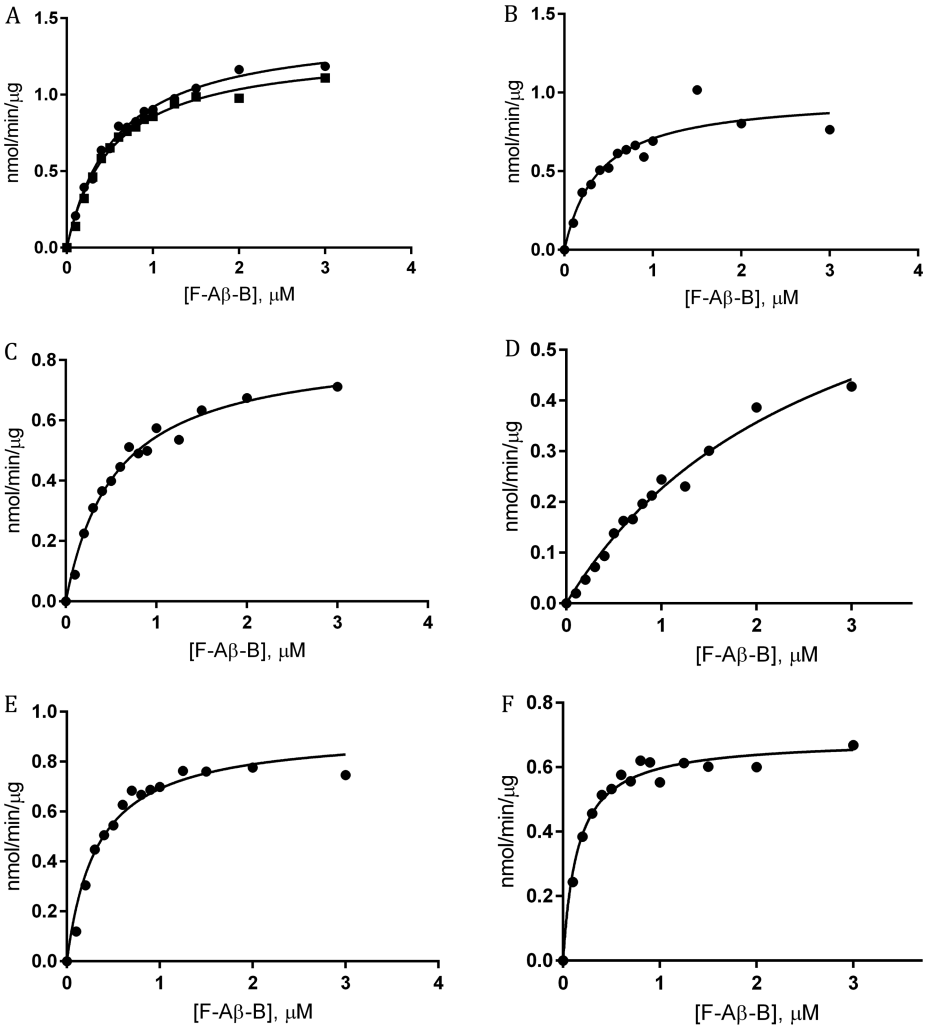

Figure 1. Degradation kinetics of the fluorescein-Aβ_{40}-biotin compound obtained with (A) wild-type IDE (two experiments) and mutants (B) IDE^{S137A}, (C) IDE^{K364A}, (D) IDE^{D426A}, (E) IDE^{F807A}, and (F) IDE^{K898A}.

values relative to that of wild-type IDE (Table S3). To improve the precision in obtaining the K_m and k_{cat} values, the kinetic parameters of substrate degradation were determined by assaying degradation in a range of 0.1−3 μM Aβ. The data were collected in smaller, 0.1 μM, incremental steps between 0 and 1 μM substrate peptide and in 0.5 μM increments for concentrations of the substrate between 1 and 3 μM. The K_m values for wild-type IDE were found to be equal to 0.55 ± 0.02 μM.

It is important to note the K_m value obtained here is 1.5-fold lower than that of a previous report by Leissring et al.[46] Because IDE is known to act only on a monomeric form of Aβ,[49] the observed difference in the K_m value could result from the difference in a fraction of aggregated Aβ forms present in the assay. In their preparation for quantitative kinetic determinations, Leissring et al. removed aggregated Aβ from the peptide solution using ultracentrifugation. While this method removes fibrillary Aβ, it is not 100% effective in producing an Aβ solution free of oligomeric forms. Utilized in this study, ammonium hydroxide pretreatment of Aβ followed by its resuspension with sodium hydroxide was shown to result in an Aβ solution that is largely monomeric.[43] Indeed, incubation of Aβ with the excess of IDE led to complete degradation of the peptide (not shown), indicating that it was present entirely in a monomeric form.

Kinetic parameters for cleavage of Aβ by IDE^{WT} and IDE mutants obtained in two independent experiments are summarized in Figure 1, Figure S4, and Table 1. The strongest effect was observed for the IDE^{K898A} mutant, for which we obtained a 3.6-fold lower K_m (in the first experiment). The rate of substrate turnover (k_{cat}) for IDE^{K898A} was reduced 2-fold relative to that of wild-type IDE, resulting in an overall change in k_{cat}/K_m equal to 1.8. The IDE^{F807A} and IDE^{S137A} mutants also reveal a decreased K_m (1.7- and 1.4-fold, respectively, in the first experiment; close numbers in the second experiment) compared to that of IDE^{WT}. The catalytic activity (k_{cat}/K_m) of the IDE^{F807A} and IDE^{S137A} mutants is similar to that of IDE^{WT}. The IDE^{K364A} mutant shows the same K_m (0.55 ± 0.03 μM) as the IDE^{WT} and 1.6-fold reduction in its k_{cat}, leading to values lower than the wild-type catalytic efficiency (Table 1). The IDE^{D426A} mutant reveals a 5-fold higher K_m and a 1.6-fold lower k_{cat}, which result in the 8-fold decrease in its catalytic efficiency. Considering the rather moderate increase in IDE^{K898A} activity, we performed the second experiment on Aβ degradation (Figure S4 and Table 1, second experiment). We confirmed the increase of IDE^{K898A} activity, as well as lower

DOI: 10.1021/acs.biochem.6b00783
Biochemistry 2017, 56, 228−239

Table 1. Kinetic Parameters of Fluorescein-Aβ_{40}-Biotin Degradation by the Wild-Type IDE and Its Mutants

protein	K_m (μM)	V_{max} (nM min^{-1} μg^{-1})	k_{cat} (min^{-1})	k_{cat}/K_m (M^{-1} min^{-1})
		Experiment 1		
WT1	0.56 ± 0.02	1.44 ± 0.02	165 ± 3	2.9×10^8
WT2	0.53 ± 0.02	1.31 ± 0.02	151 ± 2	2.9×10^8
S137A	0.39 ± 0.05	0.98 ± 0.05	113 ± 5	2.9×10^8
K364A	0.55 ± 0.03	0.85 ± 0.02	98 ± 2	1.8×10^8
D426A	2.7 ± 0.3	0.85 ± 0.05	98 ± 6	0.4×10^8
F807A	0.33 ± 0.03	0.93 ± 0.02	107 ± 3	3.2×10^8
K898A	0.15 ± 0.01	0.69 ± 0.01	79 ± 1	5.2×10^8
		Experiment 2		
WT1	0.63 ± 0.05	1.77 ± 0.05	204 ± 6	3.2×10^8
WT2	0.60 ± 0.04	1.80 ± 0.05	207 ± 5	3.4×10^8
S137A	0.55 ± 0.04	2.02 ± 0.06	232 ± 7	4.3×10^8
K364A	0.63 ± 0.05	1.50 ± 0.04	173 ± 5	2.7×10^8
D426A	2.0 ± 0.4	0.95 ± 0.10	109 ± 12	0.5×10^8
F807A	0.42 ± 0.03	1.57 ± 0.03	181 ± 4	4.3×10^8
K898A	0.28 ± 0.03	1.15 ± 0.03	133 ± 4	4.8×10^8

K_m values in the cases of IDE^{S137A}, IDE^{F807A}, and IDE^{K898A} mutants as in experiment 1 (Figure 1 and Table 1).

It has been shown elsewhere that IDE readily undergoes dimerization, which, in turn, can allosterically regulate IDE's catalytic activity.[14] Binding of IDE to other cellular proteins was also shown to be an "intermolecular" allosteric trigger, albeit activating the degradation of only short peptides.[14] Therefore, one has to further prove that given the dimeric form of IDE used here, selected mutations can allosterically act as intramolecular switches, shifting an equilibrium toward the open state and providing access to the long substrate and its binding to the catalytic sites and exosites. This hypothesis could be corroborated, for example, if the intramolecular mutations would not affect degradation of the short peptide, the binding of which to the catalytic site does not depend on the open and closed states of the IDE.

To this end, we investigated whether the mutations introduced into IDE affected its activity toward a short synthetic peptide, Abz-GGFLRKHGQ-EDDnp. In agreement with previous reports showing that smaller peptide substrates display binding affinities for IDE lower than those of larger peptides,[37] the K_m for Abz-GGFLRKHGQ-EDDnp was found to be 33.2 ± 3 μM. None of the investigated IDE mutants reveal an affinity for the short substrate higher than that of the wild-type enzyme (Figure 2 and Table 2). The IDE^{S137A} and IDE^{K364A} mutants showed K_m values very similar to that of wild-

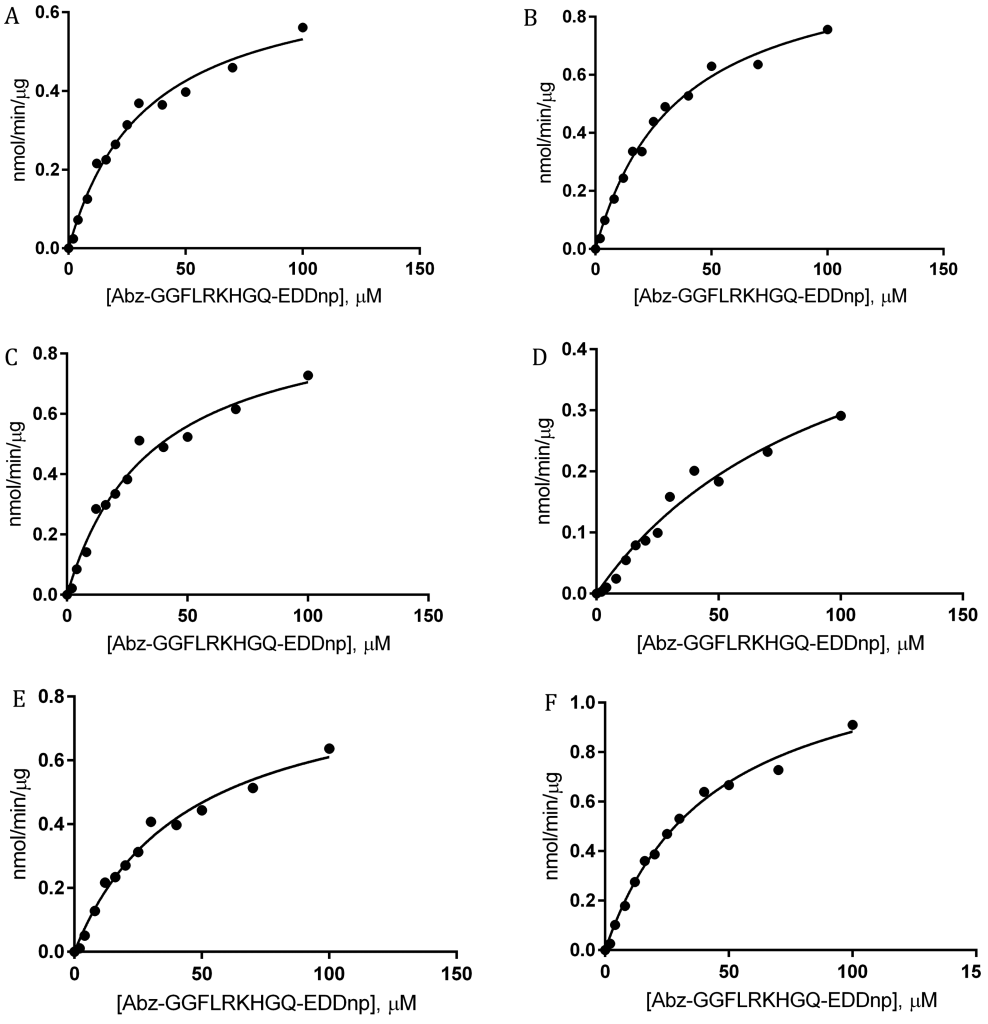

Figure 2. Degradation kinetics of the Abz-GGFLRKHGQ-EDDnp obtained with (A) wild-type IDE (two experiments) and mutants (B) IDE^{S137A}, (C) IDE^{K364A}, (D) IDE^{D426A}, (E) IDE^{F807A}, and (F) IDE^{K898A}.

DOI: 10.1021/acs.biochem.6b00783
Biochemistry 2017, 56, 228−239

Table 2. Kinetic Parameters of Abz-GGFLRKHGQ-EDDnp Degradation by Wild-Type IDE and Its Mutants

protein	K_m (μM)	V_{max} (nM min^{-1} μg^{-1})	k_{cat} (min^{-1})	k_{cat}/K_m (M^{-1} min^{-1})
WT	33 ± 3	0.71 ± 0.03	82 ± 4	2.5 × 10^6
S137A	35 ± 4	1.02 ± 0.06	118 ± 7	3.3 × 10^6
K364A	35 ± 4	0.95 ± 0.05	110 ± 6	3.1 × 10^6
D426A	103 ± 21	0.59 ± 0.08	68 ± 9	6.6 × 10^5
F807A	44 ± 4	0.88 ± 0.04	101 ± 5	2.3 × 10^6
K898A	43 ± 3	1.26 ± 0.04	145 ± 5	3.4 × 10^6

type IDE, while slightly higher K_m values were observed for the IDE^{F807A} and IDE^{K898A} mutants. In case of Aβ substrate, on the contrary, the IDE^{S137A} (experiment 2, Table 1), and IDE^{F807A} mutants showed a moderate increase (1.2−1.4-fold) in k_{cat}/K_m relative to that of IDE^{WT}, while for the IDE^{K898A} mutant, k_{cat}/K_m increased 1.5−1.8-fold (Table 1). The IDE^{D426A} mutant shows in case of short peptide a significant (3.1-fold) increase in K_m relative to that of IDE^{WT}, which together with a slight decrease in k_{cat} leads to a 3.8-fold reduction in the catalytic efficiency of the IDE^{D426A} mutant, same as for Aβ substrate. Therefore, we can conclude that the mutation D426A is damaging for IDE's activity. Taken together, these data demonstrate that selected mutations in IDE lead to a decreased K_m (IDE^{S137A}, IDE^{F807A}, and IDE^{K898A}) and an improved catalytic efficiency (IDE^{K898A}) toward Aβ. The absence of the effect of mutations in the case of Abz-GGFLRKHGQ-EDDnp emphasizes the mechanistic differences in processing of longer and shorter peptides by IDE.

Allosteric Free Energy Calculations. Here, we use a recently proposed structure-based statistical−mechanical approach to estimate the causality and energetics of allosteric effects caused by mutations.[41] To estimate the whole range of possible changes in allosteric free energy as a result of a generic mutation, two types of mutations were computationally considered (see Modeling the Allosteric Free Energy Caused by Mutations for a definition of UP and DOWN mutation types): (i) mutations that mimic the overstabilization of the residue network of contacts (UP mutation, force constant scaling factor α = 100, eq 6) and (ii) mutations that mimic the disruption of the residue's network of contacts (DOWN mutation, force constant scaling factor $\alpha = 10^{-5}$, eq 6). In particular, to draw conclusions about the effect of a mutation, we look at the double allosteric free energy difference resulting from UP and DOWN mutations (see eqs 10−12). First, we analyzed the effects of allosteric mutations by calculating per-domain allosteric free energies of IDE. Second, the allosteric effects were calculated per site for the catalytic site (residues 141, 332, 339, 341, 361, 363, 609, 824, and 831) and other parts of IDE crucial for its function: the exosite (residues 336−342 and 359−363) and substrate recognition (199 and 202) and Zn2$^+$-binding (108, 112, and 189) sites.

The data for allosteric free energy calculated for the four IDE domains are listed in Table 3 and Table S4 and illustrated in Figure 3. The per-residue allosteric free energies are illustrated in Figure 3 as a color map of the IDE's protein surface separately for UP and DOWN mutations. All the effects are stronger in the calculations with UP mutations. Therefore, here and below, the effect of the corresponding mutation is expressed via the difference between the free energy change upon an overstabilizing mutation and a destabilizing one: $\Delta\Delta g^{MUT}_{residue} = \Delta g^{\uparrow MUT}_{residue} - \Delta g^{\downarrow MUT}_{residue}$. The intuitive meaning of this quantity is the change in a protein's dynamics upon mutation of the residue that results in the strongest interactions of this residue with the rest of protein compared to a mutation that eliminates the interactions existing between the residue and the protein. It should be noted that all the values of free energy changes are given as averaged values over the residues belonging to the corresponding domains and/or sites. The minimal change in the overall protein's stability of IDE (see $\Delta\Delta g^{MUT}_{protein}$ in Materials and Methods) is observed for S137A and K898A ($\Delta\Delta g^{S137}_{protein}$ = −10.02 kcal/mol, and $\Delta\Delta g^{K898}_{protein}$ = −6.63 kcal/mol), whereas the largest change is observed for F807A ($\Delta\Delta g^{F807}_{proteen}$ = −13.05 kcal/mol). The large change in the stability of the D426A mutant ($\Delta\Delta g^{D426}_{protein}$ = −12.19 kcal/mol) is a possible reason for detrimental effect of this mutation. The S137A and K898A mutants are mutants that lead to the decrease in K_m (Figure 1, Figure S4, and Table 1). While the F807A mutant also shows a decrease in its K_m, the large change in the protein's stability associated with this mutation presumably prevents the activation of IDE^{F807A}.

Table 3. Allosteric Free Energies (per residue) or the Work Exerted in Four Domains (work performed by residues of these domains) as a Result of the Corresponding Mutations[a]

residue	protein kcal/mol	domain 1 kcal/mol	domain 2 kcal/mol	domain 3 kcal/mol	domain 4 kcal/mol
Ser137	−10.02	0.1	−0.11	−0.27	0.13
Lys364	−10.82	0.00	0.27	−0.12	−0.15
Asp426	−12.19	−0.05	−0.11	0.09	0.00
Phe807	−13.05	−0.07	−0.17	−0.05	0.17
Lys898	−6.63	0.03	−0.07	−0.03	0.01

[a]Starting form two extreme scenarios, the overstabilizing mutations (UP mutation, force constant scaling factor α = 100, $\Delta g^{\uparrow MUT}_{residue}$) and the contact-eliminating mutations (DOWN mutation, force constant scaling factor $\alpha = 10^{-5}$, $\Delta g^{\downarrow MUT}_{residue}$), the equation $\Delta\Delta g^{MUT}_{residue} = \Delta g^{\uparrow MUT}_{residue} - \Delta g^{\downarrow MUT}_{residue}$ (in kilocalories per mole) estimates the allosteric effect of a mutation. The "protein" column shows changes in the free energy of the whole protein as a result of mutation, obtained form Hessian matrices of the protein's free and bound forms.

Further details of the IDE's activity regulation emerge from the analysis of the mutations' effects calculated for the individual domains and sites involved in the IDE's function. Figure 4 schematically shows the interplay of the mutational effects, which result in changes in the allosteric free energy on the level of the corresponding domains and sites (see eq 11 in Materials and Methods). Mutations S137A and K898A lead to increased dynamics of domains D1 and D4 (Table 3), and the F807A mutation results in the increased dynamics of domain D4 (Table 3). At the same time, these mutations stabilize domains D2 and D3. Mutations K364A and D426A do not significantly affect the dynamics of domains D1 and D4 (except D426 that decreases D1's dynamics). These mutations also have a mixed effect on the dynamics of domains D2 and D3 (Table 3 and Figure 4). All of this information may serve as an indication that increased dynamics of domains D1 and D4 along with the stability of domains D2 and D3 are important for the substrate affinity and catalytic activity of IDE. Considering sites involved in IDE function, mutations D426A, F807A, and K898A lead to stabilization of all (substrate recognition, Zn^{2+}-binding, and catalytic sites and the exosite) sites involved in function, whereas the S137A mutation stabilizes all but the Zn^{2+}-binding site. The K364A mutation destabilizes the catalytic site and the exosite (Table 4, Table S5, and Figure 4). The D426A mutation stabilizes all the sites

DOI: 10.1021/acs.biochem.6b00783
Biochemistry 2017, 56, 228−239

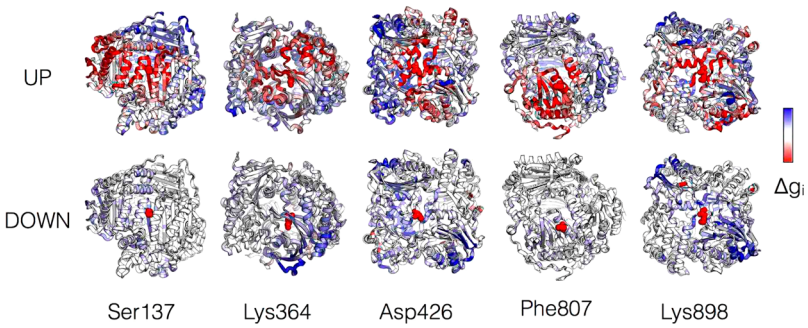

Figure 3. Allosteric free energies exerted by residues of IDE mutants investigated in the work. Two extreme scenarios are explored in this work and illustrated here: the overstabilizing mutations (UP mutation, force constant scaling factor $\alpha = 100$, $\Delta g_{residue}^{\uparrow MUT}$) and the contact-eliminating mutations (DOWN mutation, force constant scaling factor $\alpha = 10^{-5}$, $\Delta g_{residue}^{\downarrow MUT}$). The red to blue scale shows the range of the stabilization−relaxation effects caused by corresponding mutations. UP mutations typically result in stronger effects (for details, see the description in the text and the data in Tables 3 and 4, as well as in Tables S4 and S5).

mentioned above; however, the Zn^{2+}-binding site is stabilized much more strongly ($\Delta\Delta g_{Zn^{2+}}^{D426} = -0.23$ kcal/mol) than it is by other mutations, which is presumably a reason for the strongly reduced catalytic activity of IDE^{D426A} (Figure 1, Figure S4, and Table 1).

Overall, modeling of allosteric mutations shows that dynamics of domains and the stability of sites involved into binding and degradation are important for IDE's activity. The opening of the cleft is pivotal for allowing access to the catalytic and regulatory sites.[7] Because the K_m for the Aβ substrate is lower than for the wild type (Table 1), one can conclude that mutations S137A, F807A, and K898A are advantageous because they lead to increased dynamics of domains D1 and D4 (Table 3 and Table S4). At the same time, domains D2 and D3 are stabilized as a result of the mutations mentioned above, presumably providing the optimal configuration of the catalytic site and the exosite that includes residues from these domains. The stability of all sites involved in binding and degradation is important for the efficient function of IDE (Figure 4), though they should not be overstabilized, which does happen with exosites in IDE^{S137A} and IDE^{F807A} and the Zn^{2+}-binding site in IDE^{D426A}.

DISCUSSION

The specificity of the IDE's functional modulation is determined by its structure that resembles a clamshell[34] in which the substrate forms β-sheet contacts with β-strands of IDE.[35] There are several well-documented indications that disruption of contacts between the IDE-N and IDE-C domains[7,34] can turn IDE into the open state and upregulate its catalytic activity. Allosteric modulation of the IDE's activity described in many works[8,10,12,15,16,35−37] can apparently be caused by chemical modification (acrylation[10]) or binding of polyanions and/or anions,[11−13] peptides,[15,18,37] and small molecules[35,36] bound to different distal sites. It has also been shown that mutations in distal sites can yield the allosteric mode of activity regulation.[9,11,12,15,16,33]

Here, we investigated what mutations can promote a conformational change from the closed to open conformation, increasing, as a result, the substrate affinity and the catalytic activity of IDE. We experimentally analyzed five mutations of interest that were selected on the basis of computational analysis supported by previous knowledge obtained from the literature. Specifically, Ser137, Lys364, Asp426, and Lys898 were chosen because of the high residual binding leverage, a characteristic that reflects the effect of the residue on the dynamics of the whole protein and, therefore, on the allosteric signaling in this protein. All these residues are located in the interfaces between the IDE's domains and, thus, are involved in the domain dynamics as a result of the domain-level conformational changes. Phe807 reveals very low binding leverage and works as a local hydrophobic stabilizer of domain D4. Hence, we made an assumption that mutation of Phe807 could affect the IDE's dynamics. It is noteworthy that the involvement of residue K898[11,16] in allosteric signaling in the IDE was also hypothesized elsewhere.

The experimental verification of the mutations mentioned above was aimed at (i) exploring potential effects of mutations on the binding affinity and catalytic activity of the IDE and (ii) analyzing the dependence of substrate binding and degradation on the type and/or size of the substrate. Two substrates, amyloidogenic Aβ and short Abz-GGFLRKHGQ-EDDnp peptides, were used to achieve these goals. We observed an increase of the affinity for Aβ in three mutants (IDE^{S137A}, IDE^{F807A}, and IDE^{K898A}) and a 1.8-fold [1.5-fold in the second experiment (Table 1)] higher catalytic activity of IDE^{K898A}. The catalytic activity of IDE^{F807A} is only slightly increased compared to that of the wild type, and it is also approximately the same in the case of the IDE^{S137A} mutant. The K364A mutation did not change the affinity of the IDE for Aβ and decreased the catalytic activity of the protein. We also found that the D426A mutation diminishes the IDE's activity in both experiments (Figure 1, Figure S4, and Table 1).

Our recently developed structure-based statistical−mechanical model[41] was applied to estimate the effect of a mutation on protein dynamics and the allosteric signaling. In this implementation of the model, we calculate allosteric free energies in cases of contact-disrupting (DOWN mutations) and contact-enhancing mutations (UP mutations). We quantify an effect of mutation via the difference between the allosteric free energies of UP and DOWN mutations. This calculation quantifies an effect of allosteric mutations on the overall protein dynamics and energetics, which, in turn, determines the time span of the active and inactive protein states and their transitions.

One can briefly summarize results obtained with the model (Table 3, Table 4, and Tables S4 and S5) in relation to effects of mutations on IDE's activity observed in experiment (Figure 1, Figure S4, and Table 1). Analysis of the data schematically presented in Figure 4 suggests that the following factors are

DOI: 10.1021/acs.biochem.6b00783
Biochemistry 2017, 56, 228−239

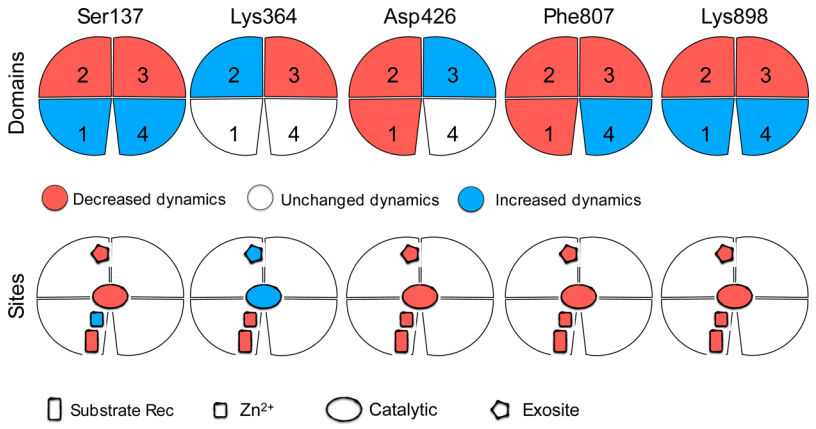

Figure 4. Schematic representation of the allosteric free energy change observed via the structure-based statistical−mechanical model in four domains and function-relevant sites of IDE. The figure illustrates that increased dynamics (blue) of domains D1 and D4 is important for the accessibility of the sites and substrate binding. The stability (red) of domains D2 and D3 secures binding and degradation at the exosite and catalytic site. The stability of all function-relevant sites is important for efficient binding and degradation of the Aβ substrate.

important for the catalytic activity of IDE: (i) dynamics of domains D1 and D4, which provides access of the substrate to the binding and catalytic sites, (ii) stability of domains D2 and D3, which secures efficient binding of the Aβ substrate to the exosite and the catalytic site, and (iii) stability of all sites involved in binding and degradation, albeit sites should not be overstabilized. The combination of these factors points to K898A as the best mutation candidate, in agreement with the increased catalytic activity observed in the experiment (Figure 1, Figure S4, and Table 1). The next two options are S137A and F807A (Table 1 and Figure 4): they obey almost all conditions described above besides the lack of stabilization of the Zn^{2+}-binding site in the case of S137A and decreased dynamics of domain D1 in IDE^{F807A}. Therefore, despite the lower K_m values observed for both mutations, the catalytic activity of mutated proteins is not improved (Figure 1, Figure S4, and Table 1). Two other mutations, neutral K364A and unfavorable D426A, lead to suboptimal dynamics of IDE's domains complemented by overstabilization of the Zn^{2+}-binding site in IDE^{D426A} and destabilization of the exosite and catalytic site in the case of IDE^{K364A}.

It was proposed elsewhere that short substrates can be degraded more efficiently upon dimerization of IDE or its interactions with other cellular proteins that play a role in intermolecular allosteric triggers.[14] In this case, intermolecular allosteric mutations in dimeric IDE should not increase the degradation efficacy of short peptides. Our results show that none of the tested mutations resulted in a significant increase in IDE activity against the short peptide substrate Abz-GGFLR-KHGQ-EDDnp. Even mutations F807A and K898A, which are the most efficient in increasing the binding affinity and activity against the Aβ amyloid peptide, affect the kinetic parameters only marginally in the case of the short peptide Abz-GGFLRKHGQ-EDDnp. The lower affinity of short peptides obtained in experiment and stabilization of the catalytic and regulatory sites as a result of activating mutations prompts us to reach the conclusion that the processes of binding and degradation are tightly connected. In other words, all the relevant sites, the catalytic, Zn^{2+}-binding, and substrate recognition sites and the exosite, should interact with the substrate as it happens in efficient degradation of $A\beta_{40}$. The stabilization of catalytic and regulatory sites observed *in silico* (see the negative values of the allosteric free energy change in Table 4 and Table S5) corroborates the importance of the stable interactions between the substrate and corresponding sites.

Table 4. Allosteric Free Energies (per residue, kilocalories per mole per residue) in Catalytic, Zn^{2+}, and Substrate Recognition Sites and the Exosite as a Result of the Corresponding Mutations[a]

residue	protein kcal/mol	substrate recognition site kcal/mol	Zn^{2+} binding site kcal/mol	catalytic site kcal/mol	exosite kcal/mol
Ser137	−10.02	−0.07	0.09	−0.03	−0.18
Lys364	−10.82	−0.02	−0.04	0.1	0.2
Asp426	−12.19	−0.09	−0.23	−0.04	−0.01
Phe807	−13.05	−0.06	−0.08	−0.06	−0.12
Lys898	−6.63	−0.1	−0.09	−0.04	−0.03

[a]The "protein" column lists changes in the free energy of the whole protein as a result of mutation. Other columns designate sites under investigation.

CONCLUSIONS

Our motivation for this work was twofold. First, we wanted to verify the existence of potential allosteric mutations that would open a perspective for activation of IDE toward amyloidogenic substrates. Second, we aimed to explore the validity of our theoretical approaches in terms of allosteric regulation as a framework for predicting and analyzing the effect of allosteric mutation at a single-residue level. The combination of computational analysis and experimental verification implemented here revealed a fine balance between the stability and dynamics on the level of individual residues, functionally relevant sites, and structural units of different scales involved in IDE function. IDE^{K898A} showed a higher efficacy of $A\beta_{40}$ degradation, corroborating that relevant mutations in distal sites can increase the IDE activity. Because Aβ clearance rather than overproduction is impaired in the common late-onset Alzheimer's disease and intraneuronal Aβ accumulation precedes extracellular Aβ deposition, one can expect that IDE specifically activated toward Aβ degradation would be beneficial for the treatment of AD. Relatively weak but reproducible activation observed for the IDE^{K898A} mutant shows that allosteric mutagenesis can be a feasible strategy for achieving

DOI: 10.1021/acs.biochem.6b00783
Biochemistry 2017, 56, 228−239

the activation of IDE against the amyloid peptides. At the same time, it prompts us to work toward a more efficient increase in activity. Subsequent work could start with an exploration of the list of potential mutation targets in Table S1 followed by investigation of double and multiple mutations that combine the most promising single-residue modifications. On the side of theoretical development, future efforts should be focused on the development of an all-atom model with a detailed consideration of the enthalpy change associated with allosteric signaling.

The calculation of the per-residue allosteric free energy associated with single mutations in IDE provides a quantification of the energetics of the processes taking place during allosteric signaling. Therefore, we propose that introducing the concept of "allosteric mutation" should be conducted on the basis of a rigorous characterization of the allosteric free energy changes upon mutation that affect protein function. An exhaustive screening of all possible mutations in the protein, estimation of the background effects, and extreme values of the allosteric free energies would provide the quantitative criteria for discriminating allosteric from non-allosteric mutations. Finally, analysis of allosteric mutations allows one to develop a combined theoretical−experimental strategy for predicting the effects of allosteric mutations on protein activity. We expect that this strategy of "allosteric mutagenesis", including further theoretical and experimental developments, could eventually be helpful in the analysis of any protein of interest.

■ ASSOCIATED CONTENT

Supporting Information

The Supporting Information is available free of charge on the ACS Publications website at DOI: 10.1021/acs.biochem.6b00783.

A set of potential mutation targets (Table S1), a list of primers used for mutagenesis of human IDE (Table S2), kinetic parameters used to establish the optimal range of Aβ concentrations (Table S3), complete data for the allosteric free energy exerted in IDE's domains (Table S4) and sites (Table S5), fractions of recombinant IDE corresponding to the dimeric form (Figure S1), purities of the IDE preparations estimated by Coomassie staining (Figure S2), kinetic parameters for determining the optimal range of fluorescein-Aβ_{40}-biotin concentrations for analysis of the degradation of Aβ_{40} (Figure S3), and kinetic parameters for cleavage of Aβ_{40} obtained in the second experiment (Figure S4) (PDF)

■ AUTHOR INFORMATION

Corresponding Author

*E-mail: igorb@bii.a-star.edu.sg. Phone: (65) 6478 8269. Fax: (65) 6478 9047.

ORCID

Igor N. Berezovsky: 0000-0002-3315-8483

Present Address

‖I.V.K.: Sysmex Corp., 4-4-4 Takatsukadai, Nishi-ku, Kobe, Japan 651-2271.

Notes

The authors declare no competing financial interest.

■ REFERENCES

(1) Monod, J., Changeux, J. P., and Jacob, F. (1963) Allosteric proteins and cellular control systems. *J. Mol. Biol. 6*, 306−329.

(2) Guarnera, E., and Berezovsky, I. N. (2016) Allosteric sites: remote control in regulation of protein activity. *Curr. Opin. Struct. Biol. 37*, 1−8.

(3) Gunasekaran, K., Ma, B., and Nussinov, R. (2004) Is allostery an intrinsic property of all dynamic proteins? *Proteins: Struct., Funct., Genet. 57*, 433−443.

(4) Berezovsky, I. N. (2013) Thermodynamics of allostery paves a way to allosteric drugs. *Biochim. Biophys. Acta, Proteins Proteomics 1834*, 830−835.

(5) Mitternacht, S., and Berezovsky, I. N. (2011) Coherent conformational degrees of freedom as a structural basis for allosteric communication. *PLoS Comput. Biol. 7*, e1002301.

(6) Duckworth, W. C., Bennett, R. G., and Hamel, F. G. (1998) Insulin degradation: progress and potential. *Endocr. Rev. 19*, 608−624.

(7) Shen, Y., Joachimiak, A., Rosner, M. R., and Tang, W. J. (2006) Structures of human insulin-degrading enzyme reveal a new substrate recognition mechanism. *Nature 443*, 870−874.

(8) Ciaccio, C., Tundo, G. R., Grasso, G., Spoto, G., Marasco, D., Ruvo, M., Gioia, M., Rizzarelli, E., and Coletta, M. (2009) Somatostatin: a novel substrate and a modulator of insulin-degrading enzyme activity. *J. Mol. Biol. 385*, 1556−1567.

(9) Im, H., Manolopoulou, M., Malito, E., Shen, Y., Zhao, J., Neant-Fery, M., Sun, C. Y., Meredith, S. C., Sisodia, S. S., Leissring, M. A., and Tang, W. J. (2007) Structure of substrate-free human insulin-degrading enzyme (IDE) and biophysical analysis of ATP-induced conformational switch of IDE. *J. Biol. Chem. 282*, 25453−25463.

(10) Neant-Fery, M., Garcia-Ordonez, R. D., Logan, T. P., Selkoe, D. J., Li, L., Reinstatler, L., and Leissring, M. A. (2008) Molecular basis for the thiol sensitivity of insulin-degrading enzyme. *Proc. Natl. Acad. Sci. U. S. A. 105*, 9582−9587.

(11) Noinaj, N., Song, E. S., Bhasin, S., Alper, B. J., Schmidt, W. K., Hersh, L. B., and Rodgers, D. W. (2012) Anion activation site of insulin-degrading enzyme. *J. Biol. Chem. 287*, 48−57.

(12) Song, E. S., Daily, A., Fried, M. G., Juliano, M. A., Juliano, L., and Hersh, L. B. (2005) Mutation of active site residues of insulin-degrading enzyme alters allosteric interactions. *J. Biol. Chem. 280*, 17701−17706.

(13) Song, E. S., Juliano, M. A., Juliano, L., Fried, M. G., Wagner, S. L., and Hersh, L. B. (2004) ATP effects on insulin-degrading enzyme are mediated primarily through its triphosphate moiety. *J. Biol. Chem. 279*, 54216−54220.

(14) Tang, W. J. (2016) Targeting Insulin-Degrading Enzyme to Treat Type 2 Diabetes Mellitus. *Trends Endocrinol. Metab. 27*, 24−34.

(15) Noinaj, N., Bhasin, S. K., Song, E. S., Scoggin, K. E., Juliano, M. A., Juliano, L., Hersh, L. B., and Rodgers, D. W. (2011) Identification of the allosteric regulatory site of insulysin. *PLoS One 6*, e20864.

(16) Song, E. S., Ozbil, M., Zhang, T., Sheetz, M., Lee, D., Tran, D., Li, S., Prabhakar, R., Hersh, L. B., and Rodgers, D. W. (2015) An Extended Polyanion Activation Surface in Insulin Degrading Enzyme. *PLoS One 10*, e0133114.

(17) Fernandez-Gamba, A., Leal, M. C., Morelli, L., and Castano, E. M. (2009) Insulin-degrading enzyme: structure-function relationship and its possible roles in health and disease. *Curr. Pharm. Des. 15*, 3644−3655.

(18) Song, E. S., and Hersh, L. B. (2005) Insulysin: an allosteric enzyme as a target for Alzheimer's disease. *J. Mol. Neurosci. 25*, 201−206.

(19) Broh-Kahn, R. H., and Mirsky, I. A. (1949) The inactivation of insulin by tissue extracts; the effect of fasting on the insulinase content of rat liver. *Arch. Biochem. 20*, 10−14.

(20) Mirsky, I. A., and Broh-Kahn, R. H. (1949) The inactivation of insulin by tissue extracts; the distribution and properties of insulin inactivating extracts. *Arch. Biochem. 20*, 1−9.

(21) Malito, E., Ralat, L. A., Manolopoulou, M., Tsay, J. L., Wadlington, N. L., and Tang, W. J. (2008) Molecular bases for the recognition of short peptide substrates and cysteine-directed

DOI: 10.1021/acs.biochem.6b00783
Biochemistry 2017, 56, 228−239

modifications of human insulin-degrading enzyme. *Biochemistry 47*, 12822−12834.
(22) Kurochkin, I. V., and Goto, S. (1994) Alzheimer's beta-amyloid peptide specifically interacts with and is degraded by insulin degrading enzyme. *FEBS Lett. 345*, 33−37.
(23) Kurochkin, I. V. (1998) Amyloidogenic determinant as a substrate recognition motif of insulin-degrading enzyme. *FEBS Lett. 427*, 153−156.
(24) Kurochkin, I. V. (2001) Insulin-degrading enzyme: embarking on amyloid destruction. *Trends Biochem. Sci. 26*, 421−425.
(25) Mawuenyega, K. G., Sigurdson, W., Ovod, V., Munsell, L., Kasten, T., Morris, J. C., Yarasheski, K. E., and Bateman, R. J. (2010) Decreased clearance of CNS beta-amyloid in Alzheimer's disease. *Science 330*, 1774.
(26) Selkoe, D. J., and Hardy, J. (2016) The amyloid hypothesis of Alzheimer's disease at 25 years. *EMBO Mol. Med. 8*, 595−608.
(27) Bayer, T. A., and Wirths, O. (2010) Intracellular accumulation of amyloid-Beta - a predictor for synaptic dysfunction and neuron loss in Alzheimer's disease. *Front. Aging Neurosci. 2*, 8.
(28) Webster, C. I., Burrell, M., Olsson, L. L., Fowler, S. B., Digby, S., Sandercock, A., Snijder, A., Tebbe, J., Haupts, U., Grudzinska, J., Jermutus, L., and Andersson, C. (2014) Engineering neprilysin activity and specificity to create a novel therapeutic for Alzheimer's disease. *PLoS One 9*, e104001.
(29) Stargardt, A., Gillis, J., Kamphuis, W., Wiemhoefer, A., Kooijman, L., Raspe, M., Benckhuijsen, W., Drijfhout, J. W., Hol, E. M., and Reits, E. (2013) Reduced amyloid-beta degradation in early Alzheimer's disease but not in the APPswePS1dE9 and 3xTg-AD mouse models. *Aging Cell 12*, 499−507.
(30) Carrasquillo, M. M., Belbin, O., Zou, F., Allen, M., Ertekin-Taner, N., Ansari, M., Wilcox, S. L., Kashino, M. R., Ma, L., Younkin, L. H., Younkin, S. G., Younkin, C. S., Dincman, T. A., Howard, M. E., Howell, C. C., Stanton, C. M., Watson, C. M., Crump, M., Vitart, V., Hayward, C., Hastie, N. D., Rudan, I., Campbell, H., Polasek, O., Brown, K., Passmore, P., Craig, D., McGuinness, B., Todd, S., Kehoe, P. G., Mann, D. M., Smith, A. D., Beaumont, H., Warden, D., Holmes, C., Heun, R., Kolsch, H., Kalsheker, N., Pankratz, V. S., Dickson, D. W., Graff-Radford, N. R., Petersen, R. C., Wright, A. F., Younkin, S. G., and Morgan, K. (2010) Concordant association of insulin degrading enzyme gene (IDE) variants with IDE mRNA, Abeta, and Alzheimer's disease. *PLoS One 5*, e8764.
(31) Qiu, W. Q., and Folstein, M. F. (2006) Insulin, insulin-degrading enzyme and amyloid-beta peptide in Alzheimer's disease: review and hypothesis. *Neurobiol. Aging 27*, 190−198.
(32) Taubes, G. (2003) Neuroscience. Insulin insults may spur Alzheimer's disease. *Science 301*, 40−41.
(33) Leissring, M. A., Farris, W., Chang, A. Y., Walsh, D. M., Wu, X., Sun, X., Frosch, M. P., and Selkoe, D. J. (2003) Enhanced proteolysis of beta-amyloid in APP transgenic mice prevents plaque formation, secondary pathology, and premature death. *Neuron 40*, 1087−1093.
(34) McCord, L. A., Liang, W. G., Dowdell, E., Kalas, V., Hoey, R. J., Koide, A., Koide, S., and Tang, W. J. (2013) Conformational states and recognition of amyloidogenic peptides of human insulin-degrading enzyme. *Proc. Natl. Acad. Sci. U. S. A. 110*, 13827−13832.
(35) Kukday, S. S., Manandhar, S. P., Ludley, M. C., Burriss, M. E., Alper, B. J., and Schmidt, W. K. (2012) Cell-permeable, small-molecule activators of the insulin-degrading enzyme. *J. Biomol. Screening 17*, 1348−1361.
(36) Maianti, J. P., McFedries, A., Foda, Z. H., Kleiner, R. E., Du, X. Q., Leissring, M. A., Tang, W. J., Charron, M. J., Seeliger, M. A., Saghatelian, A., and Liu, D. R. (2014) Anti-diabetic activity of insulin-degrading enzyme inhibitors mediated by multiple hormones. *Nature 511*, 94−98.
(37) Song, E. S., Juliano, M. A., Juliano, L., and Hersh, L. B. (2003) Substrate activation of insulin-degrading enzyme (insulysin). A potential target for drug development. *J. Biol. Chem. 278*, 49789−49794.
(38) Goncearenco, A., Mitternacht, S., Yong, T., Eisenhaber, B., Eisenhaber, F., and Berezovsky, I. N. (2013) SPACER: Server for predicting allosteric communication and effects of regulation. *Nucleic Acids Res. 41*, W266−272.
(39) Mitternacht, S., and Berezovsky, I. N. (2011) Binding leverage as a molecular basis for allosteric regulation. *PLoS Comput. Biol. 7*, e1002148.
(40) Hinsen, K. (2000) *J. Comput. Chem. 21*, 79−85.
(41) Guarnera, E., and Berezovsky, I. N. (2016) Structure-Based Statistical Mechanical Model Accounts for the Causality and Energetics of Allosteric Communication. *PLoS Comput. Biol. 12*, e1004678.
(42) Rodgers, T. L., Townsend, P. D., Burnell, D., Jones, M. L., Richards, S. A., McLeish, T. C., Pohl, E., Wilson, M. R., and Cann, M. J. (2013) Modulation of global low-frequency motions underlies allosteric regulation: demonstration in CRP/FNR family transcription factors. *PLoS Biol. 11*, e1001651.
(43) Ryan, T. M., Caine, J., Mertens, H. D., Kirby, N., Nigro, J., Breheney, K., Waddington, L. J., Streltsov, V. A., Curtain, C., Masters, C. L., and Roberts, B. R. (2013) Ammonium hydroxide treatment of Abeta produces an aggregate free solution suitable for biophysical and cell culture characterization. *PeerJ 1*, e73.
(44) Perlman, R. K., and Rosner, M. R. (1994) Identification of zinc ligands of the insulin-degrading enzyme. *J. Biol. Chem. 269*, 33140−33145.
(45) Chesneau, V., and Rosner, M. R. (2000) Functional human insulin-degrading enzyme can be expressed in bacteria. *Protein Expression Purif. 19*, 91−98.
(46) Leissring, M. A., Lu, A., Condron, M. M., Teplow, D. B., Stein, R. L., Farris, W., and Selkoe, D. J. (2003) Kinetics of amyloid beta-protein degradation determined by novel fluorescence- and fluorescence polarization-based assays. *J. Biol. Chem. 278*, 37314−37320.
(47) Chagas, J. R., Juliano, L., and Prado, E. S. (1991) Intramolecularly quenched fluorogenic tetrapeptide substrates for tissue and plasma kallikreins. *Anal. Biochem. 192*, 419−425.
(48) Gershkovich, A. A., and Kholodovych, V. V. (1996) Fluorogenic substrates for proteases based on intramolecular fluorescence energy transfer (IFETS). *J. Biochem. Biophys. Methods 33*, 135−162.
(49) Vekrellis, K., Ye, Z., Qiu, W. Q., Walsh, D., Hartley, D., Chesneau, V., Rosner, M. R., and Selkoe, D. J. (2000) Neurons regulate extracellular levels of amyloid beta-protein via proteolysis by insulin-degrading enzyme. *J. Neurosci. 20*, 1657−1665.

DOI: 10.1021/acs.biochem.6b00783
Biochemistry 2017, 56, 228−239